Article:
Zeytinci, BM, Şahin, M, Güler, MA et al. (1 more author) (2021) A practical design formulation for perforated beams with openings strengthened with ring type stiffeners subject to Vierendeel actions. Journal of Building Engineering, 43. 102915. ISSN 2352-7102

https://doi.org/10.1016/j.jobe.2021.102915

A practical design formulation for perforated beams with openings strengthened with ring type stiffeners subject to Vierendeel actions.

Barış Mehmet Zeytinci[a], Mehmet Şahin[b], Mehmet Ali Güler[c,a], Konstantinos Daniel Tsavdaridis[d,*]

[a]*Department of Mechanical Engineering, TOBB University of Economics and Technology, Ankara 06560, Turkey*
[b]*Space System Division, Turkish Aerospace Industries, Ankara 06980, Turkey*
[c]*College of Engineering and Technology, American University of the Middle East, Kuwait*
[d]*School of Civil Engineering, Faculty of Engineering and Physical Sciences, University of Leeds, Woodhouse Lane, LS2 9JT, Leeds, UK*

Abstract

In this paper, the effect of ring type stiffeners on the Vierendeel mechanism of perforated beams with various opening shapes is investigated. Vierendeel mechanism causes beams to fail with four plastic hinges that occur in the vicinity of large and usually isolated web openings. The practical ring type stiffeners are used in this study to increase the mechanical strength of perforated beams. The effects of stiffener thickness and stiffener height are analyzed for different stiffener thickness to web opening diameter and stiffener height to web thickness ratios. A beam profile of UB457x152x52 and of steel grade S275 is employed. Finite element analysis is conducted with both geometric and material non-linearities to obtain the failure loads for different cases of perforated beams. Shear/moment interaction diagrams are also obtained so that they can be directly used by practicing engineers. Such interaction curves are plotted for various opening shapes with stiffeners to demonstrate the effect of stiffeners on the Vierendeel mechanism. Yield patterns of various beams with different web opening shapes and ring type stiffeners are also presented. Moreover, a design formulation is derived for direct use by engineers. This study has ultimately shown that, the stiffener's thickness and height has different shear and moment effects on the performance of perforated beams depending on the opening type and web opening diameter.

Keywords: Shear/Moment Interaction Curve, Perforated Beams, Stiffeners, Reinforcement, Vierendeel Mechanism, Nonlinear FEA

1. Introduction

Perforated beams are widely used in aerospace, ship building and construction industries. Structural engineers try to improve the geometry and the structure of perforated beams in aerospace industry, in order to optimize the weight for fuel efficiency, i.e. longer flight distance. In construction industry, longer spans are needed for free of column and flexible floors as well as integrating hydraulic and electric services; the best way to achieve this in steel frames is by using perforated beams. Because of the high demand for the optimal design of structural members using cutting edge technologies in design, materials and manufacturing processes, there is significant research on the web opening shape of perforated beams in the last decade. Several studies have been carried out for new materials and design of topologically optimized web opening shapes (circular, hexagonal, octagonal, elliptical, rectangular etc.) using computational software and additive manufacturing techniques (Tsavdaridis et al., 2015; Christensen and Klarbring, 2008; Lagaros et al., 2008; Norato et al., 2007).

*Corresponding author: K.Tsavdaridis@leeds.ac.uk
Email addresses: bzeytinci@etu.edu.tr (Barış Mehmet Zeytinci), mehmet.sahin2@tai.com.tr (Mehmet Şahin), mehmet.guler@aum.edu.kw (Mehmet Ali Güler), K.Tsavdaridis@leeds.ac.uk (Konstantinos Daniel Tsavdaridis)

Perforated beams present about six types of failure modes mainly depending on the loading type, the geometry of the beam, namely: Vierendeel or shear mechanism of the top and bottom T-sections, flexural mechanism, rupture of welded joints, Lateral Torsional Buckling (LTB), web-post buckling in shear and compression buckling. There are also other associated failure modes caused by tension, compression, shear forces and stress distributions. Most perforated beams experience three core failure modes, namely: Vierendeel mechanism (formation of four plastic hinges), flexural failure due to reduced moment capacity, and shear failure due to reduced shear capacity.

Herein, we summarize the studies conducted on perforated beams. Chung et al. (2003); Tsavdaridis and D Mello (2009); Panedpojaman et al. (2015) proposed analytical solutions for different types of web openings and verified them with finite element (FE) results. Standard circular type of web opening and other geometries, such as elliptical and elongated type web openings are analysed by Chung et al. (2003); Tsavdaridis and D Mello (2009); Tsavdaridis and D'Mello (2011, 2012a); Tsavdaridis and D'Mello (2012b); Najafi and Wang (2017) in terms of shear/moment interaction curves. Such different types of web openings showed different types of behavior that were not considered previously. Several studies under Vierendeel mechanism have been conducted on castellated and cellular beams by Lawson et al. (2006); Martin et al. (2017). Wang et al. (2014) has investigated failure of castellated beams with fillet corner web openings under Vierendeel mechanism. Experimental results for beams that fail under Vierendeel mechanism were presented by Redwood and McCutcheon (1968); Redwood (1969); Tsavdaridis and D'Mello (2012a); Tsavdaridis and D'Mello (2012b); Erdal and Saka (2013); Morkhade and Gupta (2015); Al-Dafafea et al. (2019). Lawson and Hicks (2011) published a guideline for the design of composite beams with large web openings in accordance with Eurocodes and the UK National Annexes. SCI publication P355 is one of the most recent way to follow while designing composite beams with large web openings. Lawson and Hicks (2011) researched about the failure modes of both stiffened and unstiffened perforated beams.

The stiffeners increase the section stiffness which increases the vibration frequency and reduces the deflection of the beam, depending upon the stiffener type and parameters. Thus, the stiffener does not only improve the moment and the shear capacity, but also increase SLS (serviceability limit state) and ULS (ultimate limit state) performance of the section by increasing the vibration frequency compared to unstiffened beam with openings. In particular, beams do not only fail with ULS, but also with SLS, vibrations and fire. Vibration of a beam can be produced from different internal and external sources and it is worthy of investigation. SCI publication P354 (Smith et al., 2007) is the most recent way to analyze the floor beams which fails under vibration. As noted above, beams can also fail under fire. When the beam is under fire, material properties change due to increase in temperature, which results in early failure. There are several studies in the literature that the restraint beams are analyzed using FEA in addition to the experimental fire tests (Nadjai et al., 2016, 2017; Vassart et al., 2012). Nadjai et al. (2017) investigated three fire tests for unprotected composite cellular beams that are subjected to vertical loading. Their results showed that fire has a significant effect on the maximum axial force for failure. Nadjai et al. (2016) investigated full scale composite protected and unprotected cellular beams with intumescent coating having different opening shapes and parameters. Nadjai et al. (2016) used TNO-Diana FEA software for numerical investigation and compared their FEA results with the experimental results. Two types of failure were observed in experimental fire tests namely: Vierendeel bending and Web post buckling. It was observed that intumescent coating is the most effective way to protect the beam from fire. Furthermore, the deformation of the protected composite cellular beams is less important than the unprotected beams in the case of a fire.

Other studies focus on the effect of adding stiffeners (also known as reinforcements) to different web opening shapes. In most cases these are of ring type, horizontal or vertical in shapes. In the studies of Rahal and Harding (1990); Rahal et al. (1990); Rockey et al. (1981); Xie and Chapman (2003); Xie et al. (2008) transverse stiffeners are investigated when there is no opening arrangements. Transverse stiffeners are generally the best choice to strengthen the web post of beams. Orun and Guler (2017); Al-Thabhawee and Al-Kannoon (2018) focused on ring type stiffeners for circular type web openings. Rodrigues et al. (2014); Al-Dafafea et al. (2019) examined horizontal type stiffeners that are located on top of the openings. Panedpojaman et al. (2015); Tsavdaridis and Galiatsatos (2015) studied vertical type stiffeners positioned in different locations of the perforated beam. Stanway et al. (1993) investigated intermediate stiffeners and concentrated on the behavior of a simply supported plate with single stiffener using non-linear finite element

analysis with elasto-plastic material properties. They discovered that shear forces are larger as compared to tension forces due to the application of the out-of-plane forces on the stiffener by the web. Hence, in their subsequent study (Stanway et al., 1996), they presented a validated design method based on the strength and the stiffness criteria.

Vierendeel mechanism is responsible for reducing the shear and moment capacities of the perforated beams. There are several studies in the literature that consider the effect of this mechanism on the global load carrying capacity of the beam. Chung et al. (2001) focused on the Vierendeel mechanism in steel beams with circular web openings. In the Vierendeel mechanisms, four plastic hinges are formed in the vicinity of the web openings which decrease the load capacity of the beam and locally increase the deflections. Tsavdaridis and D'Mello (2012a); Tsavdaridis and D'Mello (2012b) examined the Vierendeel mechanism of perforated beams with different standard and nonstandard web opening shapes. They investigated eleven different geometries using FE analyses and concluded that all of them exhibit same tendency. Orun and Guler (2017) examined the buckling behavior of thin-walled beams with circular web opening reinforcement under combined loadings.

A detailed literature survey was conducted in order to select the stiffener's dimensions. The strength of beams with transverse stiffeners was examined by many researchers (Xie and Chapman, 2003; Tsavdaridis and Galiatsatos, 2015; Xie et al., 2008; Rahal and Harding, 1990; Rahal et al., 1990; Rockey et al., 1981). Morkhade et al. (2020) investigated the structural behavior of the castellated beams that had vertical stiffeners, by using both FEA and experimental methods. They concluded that robustness of the castellated beam has increased compared to the conventional I-beam. Xie and Chapman (2003) examined the design of transverse stiffeners under axial forces, however no web opening arrangements are applied in their study. Tsavdaridis and Galiatsatos (2015) also studied transverse stiffeners with closely spaced web openings. Xie et al. (2008) analyzed transverse stiffeners under different loading conditions such as: pure shear, compression, pure bending and external forces from each end. Menkulasi et al. (2015) investigated the stiffeners for castellated beams under concentrated loads. Al-Thabhawee and Al-Kannoon (2018) considered castellated beams which were stiffened with ring type stiffeners. They used non-linear FE analyses to study for four different types of beams (parent I-section beam (PISB), castellated hexagonal opening steel beams (CHOB), castellated octagonal opening steel beams (COOB), and castellated octagonal opening steel beams with ring stiffeners (COOBR)). They found out that the best results in terms of load carrying capacity were obtained if COOBR type of stiffeners were used and concluded that the best result in terms of ultimate strength are achieved when t_s/d_0 ratio equals to 0.03. Moreover, the stiffener height to thickness of the web ratio (h_s/t_w) was kept constant and equal to 4 for all models. Orun and Guler (2017) investigated the buckling behavior of thin-webbed beams with ring type stiffeners that are frequently used in aircraft structures. They also used non-linear FE analyses to simulate the beams with stiffened web openings under combined actions of compression, shear and bending. The t_s/d_0 ratio varied between 0.033 and 0.15 and the stiffener to the web thickness ratio (h_s/t_w) varied between 1.5 and 4.5, similar to to the study conducted by Al-Thabhawee and Al-Kannoon (2018). Orun and Guler (2017) also provided the interaction curves for each type of loading (compression, shear, and bending) and the interaction curves for combined loading.

In this paper, perforated beams that fail under Vierendeel mechanism are examined. Various types of perforated beam geometries and web openings are studied to attain maximum mechanical strength. Although there are few studies that examine the effect of horizontal and vertical stiffeners on the Vierendeel mechanism, there are no studies in the literature that consider the effect of ring type stiffeners on the Vierendeel mechanism of perforated beams. Therefore, this paper focuses on the Vierendeel mechanism of perforated steel beams with different web opening shapes that have ring type stiffeners. Three different opening types are selected. These are the circular (opening A), elliptical (opening C) and square (opening H) shapes considered in the study of Tsavdaridis and D'Mello (2012b). Note that this study include stiffeners around the openings, whereas stiffeners were not included in the study conducted by Tsavdaridis and D'Mello (2012b).

The paper is organized as follows: In Section 2 and 3 brief information is given for Vierendeel Mechanism and stiffeners respectively. The FE Model is validated in Section 4. Shear/moment interaction curve is explained in Section 5. The results obtained from this study are discussed in Section 6. A formula was derived regarding the design recommendations based on the shear/moment interaction curves in Section 7.

Guidelines for using the formula derived in Section 7 is given in Section 8 followed by concluding remarks in Section 9.

2. Vierendeel Mechanism

Vierendeel mechanism is generally originated from the high shear forces that act on the beam and due to the lack of a solid web. In the Vierendeel type of failure mode, plastic hinges appear at four corners in the vicinity of the web opening and deform the top and bottom T-sections. When perforated steel beams are under shear load, T-sections should carry the applied shear as well as the primary and secondary moments. Primary moment is known to be the bending moment and secondary moment is known as the Vierendeel moment. The Vierendeel moment depends on the horizontal length (critical opening length) of the web opening which also defines the effective web opening area. The Vierendeel mechanism of a perforated beam can be depicted in Fig. 1.

Plastic hinges occur at the two sides of the web opening; the low moment side (LMS) and the high moment side (HMS) (see 1). Due to the formation of these plastic hinges, it is necessary to use an elastic-plastic material model and obtain more the load carrying capacity of perforated beam accurately. Since the problem involves material and geometrical non-linearity, non-linear FE analyses were carried out for finding the shear and moment capacity of the beam. It is known that web opening shape plays a significant role in the Vierendeel behavior (Tsavdaridis and D'Mello, 2011, 2012a; Tsavdaridis and D'Mello, 2012b).

3. Stiffeners

Stiffeners are used in many structural parts to improve local and global mechanical properties such as increasing stiffness and strength. Stiffeners can be used for different purposes, for example, to reduce the vibration or to alter the failure mechanism. In structural beams, different stiffeners are employed, depending on the location, direction of load, and the geometry of the stressed area. They can be connected with the beam via riveting or different welding techniques. For perforated beams, horizontal, vertical and ring type stiffeners are used. Each type has different geometrical properties and benefits. In this study, the ring type stiffeners are selected to be analysed as they have been used and known to perfectly fit the web openings, but yet to be fully examined and understood. The geometry of the ring type stiffener of this paper is presented in Fig. 2.

From the aforementioned studies in the literature about the stiffeners in section 1 , it was concluded that the two most critical ratios for selecting a suitable stiffener are the its thickness to diameter ratio t_s/d_0 and its height to thickness of the web ratio (h_s/t_w).

In this study, the t_s/d_0 ratios are selected to be 0.03, 0.05, 0.07, and 0.09 while the h_s/t_w ratio was kept constant at 2, to see the effect of stiffener thickness (t_s). In order to investigate the effect of the height of the stiffener (h_s), the h_s/t_w ratio is varied between 2 to 4, while keeping t_s/d_0constant at 0.05. The maximum t_s/d_0 ratio and the maximum h_s/t_w ratio are selected to be 0.09 and 4 respectively. Note that higher t_s/d_0 and h_s/t_w ratios are not practical.

4. Model Validation

4.1. Validation of the FE Model with Experimental Work

Despite the fact that there are not available experimental results of perforated steel beams with ring type stiffeners, modelling steel beams has been proven a very accurate and reliable practice. The current validation of FE models is satisfactory. The introduction of stiffeners will not compromise the accuracy of the steel FE models, and can be safely used for further expanding the parametric studies. FE models were validated with the experimental tests of Redwood and McCutcheon (1968), who had carried out coupon tests to the beams named as 2A and 3A. Note that, the test is an ideal example of a test producing pure Vierendeel Mechanism. Geometries and boundary conditions of the beams are provided in Fig. 3. Beam

2A and 3A sections are hybrid plated beams with the flange and web parts having different properties. The material properties are summarized in Table 1.

ANSYS 2018 was used throughout this study to compare the computational results with the experimental ones. The beams are modeled as simply supported and a line pressure along the top of the beam is used to simulate the load on the top flange. Elastic modulus and Tangent Modulus are defined to be 200 GPa and 1 GPa respectively. In the actual coupon tests, the flange and web showed different yielding stresses. A bi-linear plastic model is defined together with the bi-linear kinematic hardening rule and the von-Mises yield criterion. Different plastic material models for the web and flanges are assigned to be compatible with the experimental models. Geometric non-linearity is also used by selecting the large-displacement option in order to attain four plastic hinges in the vicinity of the web opening.

Mesh refinement is applied near the periphery of the web openings. Maximum mesh size of 20 mm is selected and a 4-noded SHELL181 element is used for modeling the Beams 2A and 3A. The manual (mapped) mesh structure near the opening can be seen in Fig. 3c. Newton-Rhapson algorithm was used to solve geometrically non-linear problem throughout this study.

FEA results of Beam 2A and 3A are shown in Figs. 3d and 3e and are in good agreement with the results of Redwood and McCutcheon (1968). Tsavdaridis and D'Mello (2012b) also used the same experiments to validate their models and the results are presented in Figs. 3d and 3e as well. Overall, the maximum bending moment and initial plastic hinge formation modeled satisfactorily. However, it can be seen that there is a slight deviation between the results of Tsavdaridis and D'Mello (2012b) and the current study. Note that the mesh size, element type, boundary conditions and the solver are not exactly the same between our results and those of Tsavdaridis and D'Mello (2012b). Moreover, mesh around the web opening is more refined in this study to capture accurate results, since it is the most critical section for Vierendeel mechanism. These kinds of differences cause minor deviations between the results.

4.2. Shear/Moment Interaction Curve Validation

Shear/Moment (V/M) interaction diagrams are employed herein to show the interactions of shear and moment actions. The interaction curves have similar patterns, and the cubic shear/moment interaction curve that is used in the literature, changes shape due to the high shear force acting in the vicinity of the perforated section. It is noticed that the reduction in shear capacity is always more significant than the reduction in the moment capacity. Shear and moment diagrams of a simply supported beam with a distributed load (w) can be seen in Fig. 4a. In Fig. 4b, a representative shear moment interaction curve is presented together with the significant drop due to the high shear near the supports.

In Fig. 4b, the x- and y- axis are the moment and shear ratios, respectively. The shear ratio is the ratio of the global shear force (V_{sd}) to the shear capacity of the perforated section ($V_{o,Rd}$). Similarly, the moment ratio is the ratio of the global moment (M_{sd}) to the moment capacity of the perforated section ($M_{o,Rd}$). Global shear force and global moment are calculated using the load (w) obtained from FEA.

For a simply supported perforated beam under a distributed load, where the opening is located at a distance (x) from the support, the global shear force and global moment can be calculated as:

$$V_{sd} = w(\frac{L}{2} - x), \tag{1}$$

$$M_{sd} = \frac{wx}{2}(L - x). \tag{2}$$

The shear, $V_{o,Rd}$ and the moment, $M_{o,Rd}$ capacities of the perforated section can be calculated as follows:

$$V_{o,Rd} = f_v A_{vo} \geq V_{sd}, \tag{3}$$

$$M_{o,Rd} = f_y W_{o,pl} \geq M_{sd}, \tag{4}$$

where

$$A_{vo} = ht_w - d_0 t_w, \tag{5}$$

$$f_v = \frac{0.577 f_y}{\gamma_{M_o}}, \tag{6}$$

$$W_{o,pl} = W_{pl} - \frac{{d_0}^2 t_w}{4}, \tag{7}$$

and h is the depth of the beam, t_w is the web thickness, d_0 is the depth/diameter of the web opening, f_y is the design yield strength of the steel, γ_{M_o} is the safety factor (taken as 1), f_v is the shear strength of the steel, W_{pl} is the plastic modulus of the section. Other variables are presented in Fig. 2.

The shear capacity formulations detailed above, do not include flange areas. Chung et al. (2001) suggested that the flange area calculation should be associated with the shear capacity formulation. Therefore, Eq. (3) becomes:

$$V_{o,Rd} = \frac{0.577 f_y}{\gamma_{M_o}} \left[(h t_w + 2(0.75 t_f^2) - d_0 t_w) \right] > V_{o,Sd}. \tag{8}$$

The coupled shear and moment ratio can then be calculated as:

$$\bar{v} = \frac{V_{sd,FEA}}{V_{o,Rd}}, \tag{9}$$

$$\bar{m} = \frac{M_{sd,FEA}}{M_{o,Rd}}. \tag{10}$$

where $V_{sd,FEA}$ and $M_{sd,FEA}$ are the shear and moment capacities obtained from FEA.

4.2.1. Beam Section Geometry

UB457×152×52 beam was selected and used throughout this paper. Three different perforation types are used namely: A (Circular), C (Elliptical), and H (Square). These are adopted from the literature (Tsavdaridis and D'Mello, 2012b). The geometries of these models are depicted in Fig. 5. The reason for selecting these three types of perforations is that they demonstrate different shear and moment capacity behaviors.

4.2.2. FE Model

For each opening type a parametrical study was carried out in order to investigate the effect of several parameters (i.e., web opening diameter and critical opening length) on the shear and moment ratio. The assumptions used in FEA model are kept similar as it was used in the FE work of Tsavdaridis and D'Mello (2012b). Boundary conditions used in the FEA model for opening A, C and H are shown in Fig. 5.

4.2.3. Validation Results

The shear/moment interaction curves are validated using the numerical study of Tsavdaridis and D'Mello (2012b). In order to do the validation using the same geometry, a web opening is positioned at a distance x from the simple support region as shown in Fig. 5. The varying positions of the web opening is listed in Table 2.

Shear/moment interaction curves for different web opening shapes for both Tsavdaridis and D'Mello (2012b) results and the ones from the current study are presented in Fig. 6. Note that the left column belongs to the results from the literature and the right column belongs to the results from the current study. The results are presented for three different web opening types (circular, elliptical, and square shapes).

According to Tsavdaridis and D'Mello (2012b), the shear/moment interaction curve for opening A (standard circular opening) follows a typical path and the beams with the largest web openings show reduced shear/moment ratios. From Figs. 6a and 6b it can be observed that the trends are similar. Elliptical type web opening shows a good agreement (see Figs. 6c and 6d). It is worth noting that beams with opening C (elliptical web openings) behave differently than the ones with standard web openings. Moreover, the beams with the largest web openings have resulted the highest shear/moment utilization ratios; due to the small critical opening length. For beams with square web openings, the trends are similar to the ones with circular web openings (see Figs. 6e and 6f).

5. Shear/moment Interaction Curve Calculation for Ring Type Stiffeners

In this section the same comparison as in the previous section is repeated, but having the ring stiffeners in place to understand their effect on the shear and moment capacities. The geometrical properties of the perforated beam with ring type stiffener was shown in Fig. 2. According to section properties, global shear force and moments of the beam with the stiffener can be calculated as:

$$V_{o,Rd,s} = \frac{0.577 f_y}{\gamma_{Mo}} \left[(h t_w + 2(0.75 t_f^2) - d_0 t_w + 2 t_s (h_s - t_w)) \right] \tag{11}$$

$$M_{o,Rd,s} = (W_{pl} - \frac{{d_0}^2 t_w}{4} + t_s (h_s - t_w)(d_0 + t_s)) \tag{12}$$

The terms $2t_s(h_s - t_w)$ and $t_s(h_s - t_w)(d_0 + t_s)$ express the shear and moment capacity contributions of the stiffeners, respectively.

After the addition of stiffeners, the shear ratio and moment ratio become:

$$\bar{v} = \frac{V_{sd,FEA}}{V_{o,Rd,s}} \tag{13}$$

$$\bar{m} = \frac{M_{sd,FEA}}{M_{o,Rd,s}} \tag{14}$$

where $V_{sd,FEA}$ and $M_{sd,FEA}$ terms are determined from FEA analysis and $V_{o,Rd,s}$ and $M_{o,Rd,s}$ terms are obtained from Eqs. (11) and (12). The FEA model for ring type stiffeners were prepared as in the validation study.

6. Results and Discussion

In this section the effect of stiffener thickness (t_s) and stiffener height (h_s) on the shear and moment interaction curves are analyzed. As it was aforementioned, only UB457 $\times$ 152 $\times$ 52 beam is presented in this study because of practical reasons. This study carries out various non-linear FEA analysis with different geometrical parameters (stiffener thickness, stiffener height, web opening diameter, web opening type, location of the opening etc.) for both stiffened and unstiffened openings. Approximately 700 successful FEA analyses are conducted herein in order to be able to draw the shear/moment interaction curves.

6.1. Effect of Stiffener Thickness (t_s)

In this subsection, we analyze the effect of stiffener thickness on the interaction curves while t_s/d_0 ratio is varied between 0 to 0.09 and h_s/t_w ratio is kept constant. We now discuss this effect for each opening type.

6.1.1. Opening A (Circular type web opening)

For opening A, shear and moment interaction curves for various t_s/d_0 ratios are plotted in Fig. 7. The range for t_s/d_0 ratios is selected to be between 0 to 0.09. Note that, when t_s/d_0 ratio is equal to 0, it means that there is no stiffener around the opening.

As mentioned before, large web openings show reduced shear/moment ratios as the shear and moment interaction curves with and without stiffeners are compared. It can be observed that this general trend is reversed when stiffeners are used. When there is no stiffener, the shear and moment capacities of the section are reduced with larger web openings. On the other hand, the shear/moment interaction curve increases when a stiffener is added, which means that the shear and moment capacities of the sections further increase in beams with large web openings. It is concluded that the contribution of the stiffener is more significant (beneficial) for larger web openings.

Shear/moment interaction curves are shown for various d_0/h ratios in Fig. 7. The failure mechanism changes after quarter of the span (point 6, $x = 1299$ mm, see Table 2) for the case where $d_0/h = 0.5$ as shown in Fig. 7a. At this point (contra-flexure point) failure mechanisms of the beam changes from the Vierendeel type to the flexural type failure. It is worth to note that the moment becomes more significant after this point with the increase of the t_s/d_0. This can be attributed to the strength contribution to the bending capacity due to the addition of the stiffener. Chung et al. (2001) also observed this phenomenon for small web openings that the proposed formulations are conservative (see Eqs. (4) and (8)). Therefore, Eqs. (4) and (8) become even more conservative with the addition of stiffeners. It is observed that stiffeners do not affect the shear/moment interaction curves of beams with small web openings, even if these are near the supports (high shear zones). However, the effect of the stiffener is significant for perforated beams for the cases $d_0/h = 0.65$ and $d_0/h = 0.75$ (see Fig. 7b and 7c). It is concluded that larger opening diameters achieve better results in terms of shear and bending strength when thicker stiffeners are used. Overall, the stress distribution in the vicinity of the web openings results in different shapes of the shear/moment interaction curves. Also, the shear capacity ($V_{o,Rd}$) is conservatively calculated which results in reduced shear ratio.

The stiffeners around the web opening have a significant contribution to the plastic moment capacity of the beam as compared to the shear capacity. This is due to the fact adding stiffeners increases the section modulus of the cross-section which in turn increases plastic moment capacity. In other words, when a stiffener is added to the web opening, the normal stress across the section decreases at the same load level. Since the regions where stiffener is added corresponds to the minimum shear stress levels at the cross-section, stiffener contribution to the shear capacity is less significant than the moment capacity.

Please note that throughout the study, moment utilization ratio exceeds 1.0 in some cases because of the addition of the stiffener, which is also observed in the studies of Tsavdaridis and D'Mello (2012b) and Chung et al. (2003), even without the stiffener. Global moment found by FEA ($M_{sd,FEA}$) is greater than the theoretical moment capacity ($M_{o,Rd,s}$), which results in higher moment ratio. $M_{sd(FEA)}$ is greater than $M_{o,Rd,s}$ because $M_{o,Rd,s}$ assumption is based on a fully plastic behavior. Since there are plastic hinges near the web openings, the stress state is rather complex. When the stress goes into plastic region near these areas, stress redistribution happens around the web opening. Our $M_{o,Rd,s}$ formulation is based on defining the cross-section near these regions as fully plastic which may result discrepancy in predicting moment capacity. The stress redistribution along the web opening section needs to be investigated in more detail.

6.1.2. Opening C (elliptical type web opening)

Shear/moment interaction curves with varying t_s/d_0 ratios are presented in Fig. 8 while the web opening diameter to the depth of the beam ratio, d_0/h is kept constant. Note that the critical opening length is set to $c = 0.75h$ for elliptical type web openings. It is observed that as stiffener thickness is increased, beams with elliptical web openings present similar shear/moment interaction behavior as the standard (circular) type web openings. It is also noted that all load carrying capacities of beams with elliptical web openings are similar and independent of the web opening size due to the shape configuration, i.e. less critical (narrow) opening length. It is found that as the elliptical openings get larger (i.e. as d_0/h increased), shear and moment utilization ratios increase (see Fig. 8). Consequently, beams with large elliptical openings (i.e. $d_0/h = 0.65$ and $d_0/h = 0.75$) now have increased shear and moment utilization ratios (i.e. the increase in denominator is less than the increase in the nominator of Eqs. (13) and (14) for all FE models, thus the ratios are increased)

Similar conclusions can be drawn for beams with any web opening size, as in beams using the standard type web openings. Again, point-6 is the contra-flexure point where the failure type changes from the Vierendeel type to the flexural type. After that contra-flexure point, when the web opening is in high moment zone, the addition of a stiffener results in higher moment ratios due to strength contribution of the stiffener to bending capacity. In addition, it is noted that moment utilization ratios are increased for larger web openings due to the addition of the stiffener. Consequently, the thicker the stiffener, the better the shear and the moment ratios for web openings with larger diameters ($d_0 = 0.65h$ and $d_0 = 0.75h$).

6.1.3. Opening H (square type web opening)

The effect of t_s/d_0 ratio on the shear/moment interaction curves can be seen in Fig. 9 for a given web opening diameter to the depth of the beam ratio, d_0/h. In this type of web opening, critical opening length is set to $c = 1.0d_0$. It is observed that the size of the critical opening length significantly affects the structural behavior. Perforated beams with the largest web opening diameter ($d_0 = 0.75h$), considerably reduced the moment utilization ratios which were found for any stiffener thickness, alike the unstiffened beams.

It is also observed that the moment utilization ratio varies more in this type of web openings and the effect of stiffener thickness on the interaction curves is more pronounced. For all web opening diameters, it is observed that the stiffener thickness affects the shear/moment interaction curves positively as the moment ratios are increased. It is concluded that all stiffened beams behave better than the unstiffened ones.

6.2. Effect of the Stiffener Height

In this subsection, we analyze the effect of stiffener height (h_s) on shear/moment utilization ratios while t_s/d_0 ratio is kept constant and h_s/t_w ratio is varied between 0 to 4.

6.2.1. Opening A (Circular type web opening)

Fig. 10 displays the shear/moment interaction curves obtained for various h_s/t_w ratios while keeping the t_s/d_0 ratio constant. For beams with small web opening diameters ($d_0 = 0.5h$), it is noticed that no improvement was observed in terms of the shear utilization ratio. The height of the stiffener does not affect the failure load of the beam when the web opening is close to the support. However the shear capacity increases due to the term ($2t_s(h_s - t_w)$) in Eq. 11. Thus, the shear utilization ratio drops for stiffened beams. The transfer of shear from zero to maximum in the vicinity of the web opening is smoother in smaller diameters. Therefore, increasing the height of the stiffener in the direction normal to the web does not affect the shear capacity but the moment capacity. In Fig. 10 (a), point-6 ($x = 1299$ mm) is the contra-flexure point where the failure mechanism changes from the Vierendeel to flexural failure. After that point, increasing the height of the stiffener changes the failure of the beam.

For perforated beams with larger web opening diameters ($d_0 = 0.65h$ and $0.75h$), the moment ratio increases, even greater than 1.0, while the shear ratio almost remains constant, since the transition from zero shear to maximum shear is sharper at perforated sections with large web openings. Increasing the height of the stiffener in the direction normal to the web does not affect significantly the shear utilization ratio since this region partly falls in the transition region where the shear stress is considerably small. It is observed that, there is not a significant improvement on the shear utilization ratios for $h_s/t_w \geq 3$. Hence it is concluded that it is not recommended to use stiffeners with larger stiffener heights in the web opening regions near the supports as it will only add extra weight without increasing the shear utilization.

6.2.2. Opening C (elliptical type web opening)

The shear/moment interaction curves for perforated beams with elliptical web openings are depicted in Fig. 11. Similar conclusions can be drawn as in the standard circular type web openings. Increasing the stiffener height does not affect the shear utilization ratio. For this type of opening, again point-6 is the contra-flexure point where failure mode changes from Vierendeel to flexural failure, and the moment utilization ratio increases; exceeds 1.0.

In Figs. 11b and 11c, it is observed that the shear utilization ratio is almost kept constant while the moment utilization ratio increases as the stiffener height is increased. For large web opening diameters, the transfer region from zero shear to maximum shear is sharper, thus the contribution of the height of the stiffener is more effective with higher h_s/t_w ratios. For $h_s/t_w \geq 3$, as in beams with circular web openings, no improvement on shear utilization ratio was observed, the same conclusion can be drawn for Openings A and C.

6.2.3. Opening H (square type web opening)

Shear/moment interaction curves are depicted in Fig. 12 for beams with square type web openings. It is concluded that the height of the stiffener affects the moment utilization ratios in all web opening

diameters. Owing to its large square web opening area (full web opening is the effective web opening area), the shear and moment ratios of perforated beams with square web opening are significantly affected by the use of stiffeners. This is mainly due to the early yielding of such perforated beams and the concentration of stresses in the sharp edge corners. Again, for $h_s/t_w \geq 3$, no improvement is observed.

6.3. Yield Patterns

Vierendeel mechanism is usually identified by the formation of four plastic hinges in the vicinity of the web openings. The plastic hinges are noticeable when the von-Mises stress distribution is plotted near the web opening. By observing the movement of the plastic hinges, the critical opening length (thus, the effective web opening area) of an opening can be determined. Panedpojaman et al. (2015) (Fig. 13a) and current study (Fig. 13b), shows a similar von-Mises stress distributions in the vicinity of circular web opening with a diameter of $d_0 = 0.5h$. It is observed that the plastic hinges that occur at the vicinity of the web opening are nearly the same. Tsavdaridis and D'Mello (2012b) also presented von-Mises stress distribution for eleven different standard and nonstandard web opening shapes with a detailed analysis. A direct comparison of the von-Mises stresses for beams with large elliptical type web openings ($d_0 = 0.8h$) is presented in Fig. 13c with the corresponding one in this study in Fig. 13d. Chung et al. (2003) obtained the von-Mises stress distribution for square type web opening (Fig. 13e). It is clear that the plastic hinges are in-line with the current study (Fig. 13f).

Please note that all the studies are carried out for the beam section UB 457×152×52. Since there was no recent study in the open literature about the elliptical type and square type web openings, Chung et al. (2003) and Tsavdaridis and D'Mello (2012b) are used in order to compare the yield patterns.

The plastic hinges formed on the top and bottom T-sections are similar for elliptical type of web opening in terms of the angular location and order of formation. Analysis for UB 457×152×52 are completed successfully for different web openings with ring type reinforcement. Yield patterns for three different type of web openings for various t_s/d_0 ratios are provided in Fig. 14 for the beams with web opening position at $x = 284$ mm and $d_0 = 0.75h$.

In Fig. 14, all of the patterns are captured using the same deformation scale for direct comparison. It is observed that the Vierendeel mechanism decreases as t_s/d_0 ratio increases. For beams with openings A and C, with the increasing stiffener thickness, the failure type changes from Vierendeel failure to vertical shear failure. Plastic hinges that are formed at the four 'corners' of the openings, disappear with ring type stiffeners owing to the better stress distribution. Plastic deformation starts to appear from the top of the web opening and spreads up to the flange, like a flexural type of failure. This results in increased failure load which causes the beam to fail later. On the other hand, von-Mises stress patterns remain in beams with square type web openings, indicating the highly stressed regions at the sharp corners despite the use of thick stiffeners due to the large critical opening length in square type openings. However, the load carrying capacity of the stiffened beams with square type web openings is improved significantly. It is observed that deflection also decreases with the increasing stiffener thickness.

6.4. Failure Modes

Von-Mises stress distributions at the web opening location ($x = 284$ mm) are presented for opening A, C and H in Fig. 15 for both unstiffened and stiffened beams. Similar conclusions can be drawn with the previous "Yield Patterns" section for all types of openings. From Fig. 15a and 15b, it can be observed that Vierendeel mode failure turns into the vertical shear failure. Application of ring type stiffeners are very useful to strengthen the area around the perforated section. This results in the increase of the failure load and the decrease in the deformation, which is also very similar for opening C (see Fig. 15c and 15d). Moreover, Vierendeel type of failure turns into vertical shear failure and the plastic hinges disappear at the vicinity of the opening and start to appear at the top and bottom T-sections. For opening H (see Fig. 15e and 15f), stress patterns that appear around the opening remains the same. 4 plastic hinges appear at four corners around the opening, however, the deformation around the web openings for ring stiffeners is significantly less compared to the unstiffened beam. Therefore, it can be concluded that application of ring stiffeners increase the failure load of the beam but does not cause a change in the failure mode.

6.5. Design Considerations

SCI publication P355 proposes a method to design a composite beam with large web openings having different kind of stiffeners such as horizontal, vertical and ring type. However, Vierendeel bending resistance was not investigated in SCI P355 for web openings reinforced with ring stiffeners. Only horizontal stiffeners for single and double sided were investigated under Vierendeel action.

Lawson and Hicks (2011) examined the failure modes of beams with different types of stiffened and unstiffened web opening configurations under web post shear buckling, bending and shear resistance as well as Vierendeel bending.

For ring type stiffeners, Lawson and Hicks (2011) studied the web post behaviour where the stiffeners were welded around the circular and rectangular web openings. It was mentioned that ring stiffeners reduce the slenderness of the web post by 30% according to the their FEA where the openings are widely spaced.

7. Design Recommendations

In the foregoing, a formulation was derived regarding the shear/moment interaction curves that are obtained in Section 6 for the practical design of the beams with ring type stiffeners. To derive a practical design formulation in terms of shear and moment, first of all, shear and moment ratios should be generated. To attain a ratio for shear and moment, global shear force and global moment should be divided with the maximum global shear force and the maximum global moment, respectively. Maximum global shear force occurs when x is equal to zero in Eq. (1), i.e., the centreline of the web opening is aligned with the support:

$$V_{sd,max} = \frac{wL}{2} \tag{15}$$

and maximum global moment occurs when $x = L/2$ in Eq. (2), i.e., centreline of the web opening is at the mid-span of the beam:

$$M_{sd,max} = \frac{wL^2}{8} \tag{16}$$

Therefore, shear and moment ratios can be calculated as:

$$v = \frac{V_{sd}}{V_{sd,max}} = 1 - 2\frac{x}{L} \tag{17}$$

$$m = \frac{M_{sd}}{M_{sd,max}} = 4\left(1 - \frac{x}{L}\right)\left(\frac{x}{L}\right) \tag{18}$$

Using Eqs. (17) and (18), the shear ratio (v) can be expressed in terms of the moment ratio (m) as;

$$v = (1 - m)^{1/2} \tag{19}$$

A generalized nondimensional shear/moment interaction curve is obtained based on a nonlinear elliptical equation (based on Eq. (19)) which represents the data generated using FEA in this study. Proposed design curves can be obtained using the equation below:

$$\overline{\overline{v_s}} = \begin{cases} \overline{v} + \left[(c_1 - m^{p_1})^{p_2} - 1\right] c_3, & \overline{v} < 0.7 \\ \overline{v}\left[c_1 - \left(\frac{m}{c_2}\right)^{p_1}\right]^{p_2}, & \overline{v} \geq 0.7 \end{cases} \tag{20}$$

where maximum coupled shear ratios ($\overline{v}$) for each type of web opening with different properties (i.e., web opening diameter, stiffener thickness and stiffener height) are provided in Table 4. Note that, p_1, p_2, c_1, c_2 and c_3 are constants that can be obtained from Tables 5, 6, 7 for $d_0/h = 0.5$, $d_0/h = 0.65$ and $d_0/h = 0.75$ respectively, for different web opening types.

It should be noted that the design recommendations given above are based on the interaction curves for a specific commonly used perforated beam section. Other typical steel sections previously studied by

Tsavdaridis and D'Mello (2012b) and Chung et al. (2003), show similar behavior according to Figures 7 - 12. Consequently, the effect of the parameters studied herein is not expected changing significantly and similar conclusions can be drawn.

To generalize the applicability of the proposed formula and retain accuracy, testing numerous sections is required. Thus it is suggested that data from the literature is acquired and an Artificial Neural Network (ANN) model is developed for the prediction of the capacity of various cellular beam sections with ring type stiffeners while maintaining a stable numerical behavior. The explicit equation that describes mathematically the ANN will be offered for easier implementation and evaluation purposes.

8. Example for Using the Formula Given in Eq. (20)

In this section we provide an example for using the formula given in Eq. (20) for a UB 457×152×52 beam with a circular type web opening (Opening A). Note that web opening diameters of $d_0 = 0.5h$, $0.65h$ and $0.75h$ and the stiffener geometrical parameters are set to $t_s/d_0 = 0.09$, $h_s/t_w = 2$ in this example. For a web opening diameter, the maximum coupled shear ratio ($\overline{v}$) and the constants used in Eq. (20) are obtained from Tables 4 - 7. The curves obtained using the formula given in Eq. (20) can be seen in Fig. 16 (solid lines in red). In order to assess the quality of curve fit, the mean values of error and COV values are calculated for the comparison of two data sets obtained from FEA and the proposed practical design formulation. Mean values of error range between 0.5-2.9% and COV values range between 2.1-6.2%. This shows that the proposed design formula fits well with the data points obtained using FEA.

For a practical design, the following design steps are suggested in order to evaluate and assess the Vierendeel capacity of the selected beam with a stiffened opening as follows:

1. Select the web opening type (A, C or H)
2. Select the web opening location, x, diameter d_0 and stiffener parameters h_s, t_s
3. Calculate the theoretical shear and moment capacity with the ring type stiffener ($V_{o,Rd,s}$, $M_{o,Rd,s}$) that are given in Eq. (11) and (12) respectively.
4. Calculate the global shear force and the global bending moment (V_{sd}, M_{sd}) that are given in Eq. (1) and (2) respectively, according to the applied load w and the hole location x.
5. Find the moment ratio ($\overline{m}$) stated in Eq. (14) by dividing the global bending moment (M_{sd}) found in step 4 with the theoretical moment capacity with the ring type stiffener ($M_{o,Rd,s}$) found in step 3.
6. Select the coupled shear ratio ($\overline{v}$) that are provided in Table 4 according to the opening type, web opening diameter and stiffener properties.
7. Select the constants that are provided in Table 5-7 according to the opening type, web opening diameter and stiffener properties.
8. Find the design coupled shear ratio $\overline{\overline{v_s}}$ using Eq. (20).
9. Multiply the design coupled shear ratio ($\overline{\overline{v_s}}$) with the theoretical shear capacity with the ring type stiffener ($V_{o,Rd,s}$) calculated in Step 3 to get ($\overline{\overline{v_s}}V_{o,Rd,s}$)
10. Check if the result found in step 9 is greater than or equal to the global shear force V_{sd} that is obtained in step 4. if $\overline{\overline{v_s}}V_{o,Rd,s} \geq V_{sd}$, the selected design have sufficient strength.
11. if $\overline{\overline{v_s}}V_{o,Rd,s} < V_{sd}$, parameters affecting the results such as opening type, applied load or the web opening diameter etc., should be changed/redesigned to attain the required mechanical strength.

9. Concluding Remarks

A non-linear FE study was carried out to understand the effect of ring type stiffeners on the shear and moment capacities as well as the Vierendeel mechanism for perforated beams with three different web opening shapes (aka circular (Opening A), elliptical (Opening C), and square (Opening H) type). Shear/moment interaction curves are compared with the results found in the literature and a design methodology is proposed for stiffened perforated beams with various standard and nonstandard web opening and of different geometric characteristics. The effect of the ring stiffener height and stiffener thickness on the shear and moment capacities was examined in detail. From the results of this study the following conclusions can be drawn:

- The larger the stiffener thickness (t_s), the higher moment utilization ratio is achieved (independent of the opening size and shape).
- Increasing the stiffener thickness to diameter ratio (t_s/d_0), the shear utilization ratio is only affected when web opening diameter is larger.
- Independent of the web opening shape, it is more effective to use a ring type stiffener when $d_0 = 0.65h$ and $d_0 = 0.75h$; the effect of the stiffeners is minimal with small openings ($d_0 = 0.5h$).
- For medium and large web opening diameters ($d_0 = 0.65h$ and $0.75h$), the moment utilization ratio increases when the height of the stiffener (h_s) increases, independent of the web opening shape.
- It is not worth to use a stiffener with bigger height when h_s/t_w ratio is equal to greater to 3.0.
- Increasing the thickness of the stiffener (t_s) is more effective than increasing the height of the stiffener (h_s) for the Vierendeel type failure.
- For beams with openings A and C, the yield patterns showed that the ring type stiffeners alter the failure mode. Beam starts to fail with vertical shear instead of Vierendeel mechanism, the plastic hinges disappear and plastic deformation starts to appear from the top of the web opening and spreads up to flange.
- For beam with opening H, the yield pattern prove that the Vierendeel type failure is dominant due to the large critical opening length and the sharp edge corners.
- For practical design two equations are derived from the shear/moment interaction curves for engineers to directly be used.
- From comprehensive parametric studies on perforated beams, it has been concluded the effect of geometric imperfections is insignificant, thus can be omitted. It should be noted that we focused in local buckling due to high shear in the vicinity of the opening in this study.

Acknowledgements

Authors would like to thank Mehmet Raif Taşdemir for his contribution to the FEA studies.

References

Al-Dafafea, T., Durif, S., Bouchaïr, A., Fournely, E., 2019. Experimental study of beams with stiffened large web openings. Journal of Constructional Steel Research 154, 149–160.

Al-Thabhawee, H.W.A., Al-Kannoon, M.A.A., 2018. Improving behavior of castellated beam by adding spacer plat and steel rings. Journal of University of Babylon 26, 331–344.

Christensen, P.W., Klarbring, A., 2008. An introduction to structural optimization. volume 153. Springer Science & Business Media.

Chung, K., Liu, C., Ko, A., 2003. Steel beams with large web openings of various shapes and sizes: an empirical design method using a generalised moment-shear interaction curve. Journal of Constructional Steel Research 59, 1177–1200.

Chung, K., Liu, T., Ko, A., 2001. Investigation on vierendeel mechanism in steel beams with circular web openings. Journal of Constructional Steel Research 57, 467–490.

Erdal, F., Saka, M.P., 2013. Ultimate load carrying capacity of optimally designed steel cellular beams. Journal of constructional steel research 80, 355–368.

Lagaros, N.D., Psarras, L.D., Papadrakakis, M., Panagiotou, G., 2008. Optimum design of steel structures with web openings. Engineering Structures 30, 2528–2537.

Lawson, R., Hicks, S., 2011. Design of composite beams with large web openings. SCI P355 .

Lawson, R., Lim, J., Hicks, S., Simms, W., 2006. Design of composite asymmetric cellular beams and beams with large web openings. Journal of Constructional Steel Research 62, 614–629.

Liu, T., Chung, K., 2003. Steel beams with large web openings of various shapes and sizes: finite element investigation. Journal of Constructional Steel Research 59, 1159–1176.

Martin, P.O., Couchaux, M., Vassart, O., Bureau, A., 2017. An analytical method for the resistance of cellular beams with sinusoidal openings. Engineering structures 143, 113–126.

Menkulasi, F., Moen, C.D., Eatherton, M.R., Kuruppuarachchi, D., 2015. Investigation of stiffener requirements in castellated beams, in: Proceedings of the Annual Stability Conference Structural Stability Research Council Nashville, Tennessee.
Morkhade, S.G., Gupta, L.M., 2015. An experimental and parametric study on steel beams with web openings. International Journal of Advanced Structural Engineering (IJASE) 7, 249–260.
Morkhade, S.G., Lokhande, R.S., Gund, U.D., Divate, A.B., Deosarkar, S.S., Chavan, M.U., 2020. Structural behaviour of castellated steel beams with reinforced web openings. Asian Journal of Civil Engineering 21, 1067–1078.
Nadjai, A., Han, S., Ali, F., Alam, N., Allam, A., 2017. Fire resistance of axial restraint composite floor steel cellular beams. Journal of Constructional Steel Research 136, 229–237.
Nadjai, A., Petrou, K., Han, S., Ali, F., 2016. Performance of unprotected and protected cellular beams in fire conditions. Construction and Building Materials 105, 579–588.
Najafi, M., Wang, Y., 2017. Behaviour and design of steel members with web openings under combined bending, shear and compression. Journal of Constructional Steel Research 128, 579–600.
Norato, J.A., Bendsøe, M.P., Haber, R.B., Tortorelli, D.A., 2007. A topological derivative method for topology optimization. Structural and Multidisciplinary Optimization 33, 375–386.
Orun, A.E., Guler, M.A., 2017. Effect of hole reinforcement on the buckling behaviour of thin-walled beams subjected to combined loading. Thin-Walled Structures 118, 12–22.
Panedpojaman, P., Thepchatri, T., Limkatanyu, S., 2015. Novel simplified equations for vierendeel design of beams with (elongated) circular openings. Journal of Constructional Steel Research 112, 10–21.
Rahal, K., Harding, J., 1990. Transversely stiffened girder webs subjected to shear loading-part 1: Behaviour. Proceedings of the Institution of Civil Engineers 89, 47–65.
Rahal, K., Harding, J., RICHMOND, B., 5400, B., 1990. Transversely stiffened girder webs subjected to shear loading-part 2: Stiffener design. Proceedings of the Institution of Civil Engineers 89, 67–87.
Redwood, R.G., 1969. The strength of steel beams with unreinforced web holes. Civil engineering and public works review 64, 559–562.
Redwood, R.G., McCutcheon, J.O., 1968. Beam tests with unreinforced web openings. Journal of the Structural Division .
Rockey, K., Valtinat, G., Tang, K., 1981. The design of transverse stiffeners on webs loaded in shear-an ultimate load approach. Proceedings of the Institution of Civil Engineers 71, 1069–1099.
Rodrigues, F., Vellasco, P.C.d.S., de Lima, L.R., de Andrade, S.A., 2014. Finite element modelling of steel beams with web openings. Engineering 6, 886.
Smith, A.L., Hicks, S.J., Devine, P.J., 2007. Design of floors for vibration: A new approach. Steel Construction Institute Ascot, Berkshire, UK.
Stanway, G., Chapman, J., Dowling, P., 1993. Behaviour of a web plate in shear with an intermediate stiffener. Proceedings of the Institution of Civil Engineers-Structures and Buildings 99, 327–344.
Stanway, G., Chapman, J., Dowling, P., 1996. A design model for intermediate web stiffeners. Proceedings of the Institution of Civil Engineers-Structures and Buildings 116, 54–68.
Tsavdaridis, K., D Mello, C., 2009. Finite element investigation of perforated steel beams with different web opening configurations, in: ICASS'09/IJSSD-Proceedings of Sixth International Conference on Advances in Steel Structures and Progress in Structural Stability and Dynamics, ICASS'09 Press. pp. 213–220.
Tsavdaridis, K.D., D'Mello, C., 2011. Web buckling study of the behaviour and strength of perforated steel beams with different novel web opening shapes. Journal of Constructional Steel Research 67, 1605–1620.
Tsavdaridis, K.D., D'Mello, C., 2012a. Optimisation of novel elliptically-based web opening shapes of perforated steel beams. Journal of Constructional Steel Research 76, 39–53.
Tsavdaridis, K.D., D'Mello, C., 2012b. Vierendeel bending study of perforated steel beams with various novel web opening shapes through nonlinear finite-element analyses. Journal of Structural Engineering 138, 1214–1230.
Tsavdaridis, K.D., Galiatsatos, G., 2015. Assessment of cellular beams with transverse stiffeners and closely spaced web openings. Thin-Walled Structures 94, 636–650.
Tsavdaridis, K.D., Kingman, J.J., Toropov, V.V., 2015. Application of structural topology optimisation to perforated steel beams. Computers & Structures 158, 108–123.
Vassart, O., Bailey, C., Hawes, M., Nadjai, A., Simms, W., Zhao, B., Gernay, T., Franssen, J.M., 2012. Large-scale fire test of unprotected cellular beam acting in membrane action. Proceedings of the Institution of Civil Engineers-Structures and Buildings 165, 327–334.
Wang, P., Ma, Q., Wang, X., 2014. Investigation on vierendeel mechanism failure of castellated steel beams with fillet corner web openings. Engineering structures 74, 44–51.
Xie, M., Chapman, J., 2003. Design of web stiffeners: axial forces. Journal of Constructional Steel Research 59, 1035–1056.
Xie, M., Chapman, J., Hobbs, R., 2008. A rational design model for transverse web stiffeners. Journal of Constructional Steel Research 64, 928–946.

List of Tables

List of Figures

Table 1: Material properties of Beam 2A and 3A

	Measured Material Strengths	Beam 2A	Beam 3A
Flange	Yield Strength, f_y (MPa)	352	311
	Tensile Strength, f_{ult} (MPa)	503	576
Web	Yield Strength, f_y (MPa)	376	361
	Tensile Strength, f_{ult} (MPa)	512	492

Table 2: Web Opening Positions (x)

Position	1	2	3	4	5	6	7	8	9	10
x [mm]	0	284	537	788	1039	1299	1573	1866	2177	2500

Table 3: Comparison of non-dimensional slenderness with Lawson and Hicks (2011) (SCI P355)

	Widely spaced openings (%)	Closely spaced openings (%)
Lawson and Hicks (2011)	30	15
Current Study	35	22

Table 4: Maximum coupled shear ratio for each type of web opening ($\overline{v}$)

	t_s/d_0	h_s/t_w	$d_0 = 0.5h$	$d_0 = 0.65h$	$d_0 = 0.75h$
Opening A	0	0	0.86	0.82	0.76
	0.03	2	0.82	0.83	0.84
	0.05	2	0.78	0.83	0.86
	0.07	2	0.77	0.84	0.89
	0.09	2	0.75	0.84	0.91
	0.05	3	0.72	0.80	0.90
	0.05	4	0.70	0.77	0.87
Opening C	0	0	0.73	0.76	0.86
	0.03	2	0.73	0.75	0.87
	0.05	2	0.7	0.81	0.89
	0.07	2	0.69	0.85	0.92
	0.09	2	0.68	0.86	0.94
	0.05	3	0.70	0.75	0.93
	0.05	4	0.61	0.75	0.88
Opening H	0	0	0.63	0.49	0.27
	0.03	2	0.65	0.52	0.33
	0.05	2	0.65	0.53	0.36
	0.07	2	0.65	0.55	0.38
	0.09	2	0.65	0.56	0.41
	0.05	3	0.69	0.60	0.42
	0.05	4	0.69	0.60	0.41

Table 5: Constants appearing in Eq. (20) for opening A, C and H for $d_0 = 0.5h$

$d_0 = 0.5h$							
	t_s/d_0	h_s/t_w	p_1	p_2	c_1	c_2	c_3
Opening A	0	0	2.19	0.36	1.00	0.96	–
	0.03	2	2.24	0.39	1.00	0.98	–
	0.05	2	2.20	0.36	1.00	0.99	–
	0.07	2	2.15	0.38	1.00	0.99	–
	0.09	2	1.55	0.33	1.00	1.00	–
	0.05	3	0.98	0.91	1.00	0.91	–
	0.05	4	1.57	0.43	1.05	1.02	–
Opening C	0	0	2.37	0.47	1.00	0.92	–
	0.03	2	2.04	0.43	1.00	1.00	–
	0.05	2	1.54	0.15	1.10	–	1.77
	0.07	2	1.35	0.29	1.10	–	0.99
	0.09	2	0.99	0.16	1.10	–	1.46
	0.05	3	1.31	0.57	1.10	1.01	–
	0.05	4	0.87	0.07	1.20	–	3.27
Opening H	0	0	1.51	0.62	1.00	–	0.64
	0.03	2	2.17	0.69	1.00	–	0.65
	0.05	2	1.15	0.37	1.10	–	0.89
	0.07	2	1.27	0.37	1.10	–	0.80
	0.09	2	1.33	0.37	1.10	–	0.78
	0.05	3	0.84	0.08	1.10	–	2.65
	0.05	4	0.79	0.08	1.10	–	2.62

Table 6: Constants appearing in Eq. (20) for opening A, C and H for $d_0 = 0.65h$.

$d_0 = 0.65h$							
	t_s/d_0	h_s/t_w	p_1	p_2	c_1	c_2	c_3
Opening A	0	0	1.54	0.42	1.10	0.94	–
	0.03	2	1.54	0.35	1.10	0.95	–
	0.05	2	1.97	0.42	1.10	1.03	–
	0.07	2	1.60	0.45	1.15	1.05	–
	0.09	2	1.68	0.41	1.15	1.06	–
	0.05	3	1.60	0.40	1.10	1.05	–
	0.05	4	1.60	0.35	1.20	1.06	–
Opening C	0	0	3.34	0.82	1.10	0.99	–
	0.03	2	3.12	0.60	1.10	1.02	–
	0.05	2	2.64	0.53	1.10	1.04	–
	0.07	2	1.88	0.45	1.10	1.05	–
	0.09	2	1.63	0.42	1.15	1.05	–
	0.05	3	4.45	0.58	1.20	1.12	–
	0.05	4	1.85	0.33	1.20	1.07	–
Opening H	0	0	2.80	0.35	1.00	–	0.46
	0.03	2	2.50	0.33	1.00	–	0.46
	0.05	2	1.60	0.14	1.10	–	0.92
	0.07	2	1.20	0.12	1.10	–	0.95
	0.09	2	1.18	0.09	1.20	–	1.48
	0.05	3	1.00	0.19	1.10	–	0.68
	0.05	4	1.20	0.18	1.20	–	0.91

Table 7: Constants appearing in Eq. (20) for opening A, C and H for $d_0 = 0.75h$.

$d_0 = 0.75h$.							
	t_s/d_0	h_s/t_w	p_1	p_2	c_1	c_2	c_3
Opening A	0	0	2.33	0.59	1.10	0.98	–
	0.03	2	2.01	0.37	1.10	0.99	–
	0.05	2	2.14	0.38	1.10	1.01	–
	0.07	2	1.80	0.36	1.10	1.02	–
	0.09	2	1.55	0.28	1.10	1.03	–
	0.05	3	1.33	0.27	1.10	1.02	–
	0.05	4	1.79	0.32	1.15	1.04	–
Opening C	0	0	1.65	0.38	1.10	0.94	–
	0.03	2	2.09	0.37	1.10	0.99	–
	0.05	2	2.23	0.37	1.10	1.02	–
	0.07	2	1.91	0.34	1.10	1.03	–
	0.09	2	1.95	0.35	1.10	1.04	–
	0.05	3	1.86	0.31	1.10	1.05	–
	0.05	4	1.51	0.39	1.20	1.04	–
Opening H	0	0	3.30	0.80	1.00	–	0.49
	0.03	2	2.14	0.01	1.00	–	16.3
	0.05	2	2.15	0.57	1.00	–	0.49
	0.07	2	3.07	0.43	1.00	–	0.39
	0.09	2	2.09	0.39	1.00	–	0.41
	0.05	3	2.70	0.47	1.00	–	0.42
	0.05	4	1.78	0.36	1.10	–	0.5

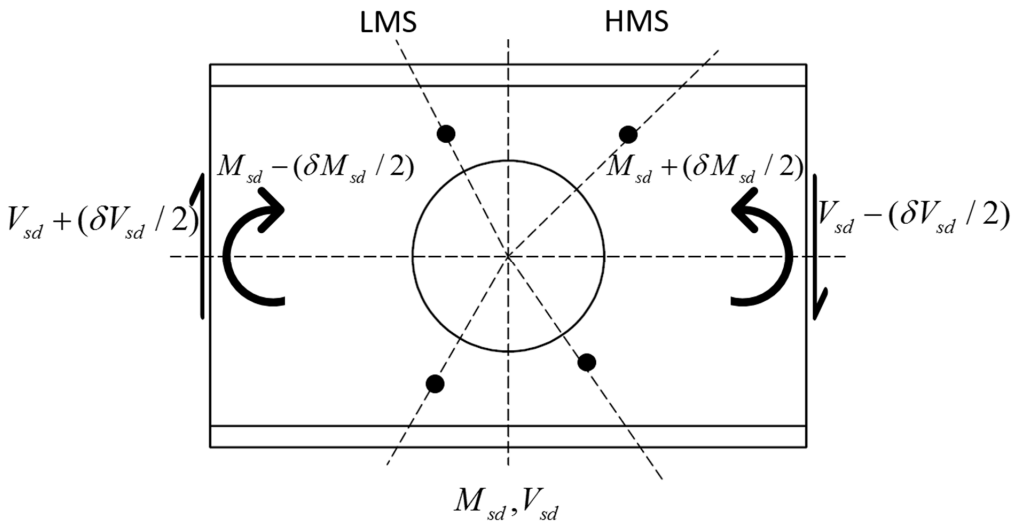

Figure 1: Vierendeel mechanism

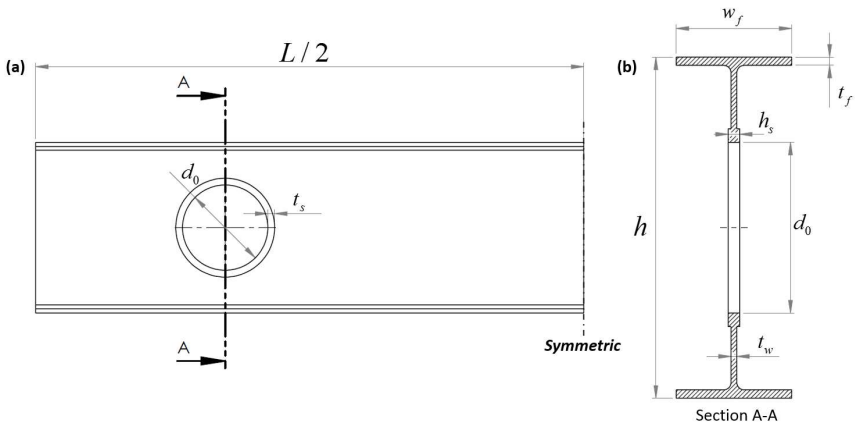

Figure 2: Section properties of I-beam with ring type stiffeners (a) front view, (b) section view

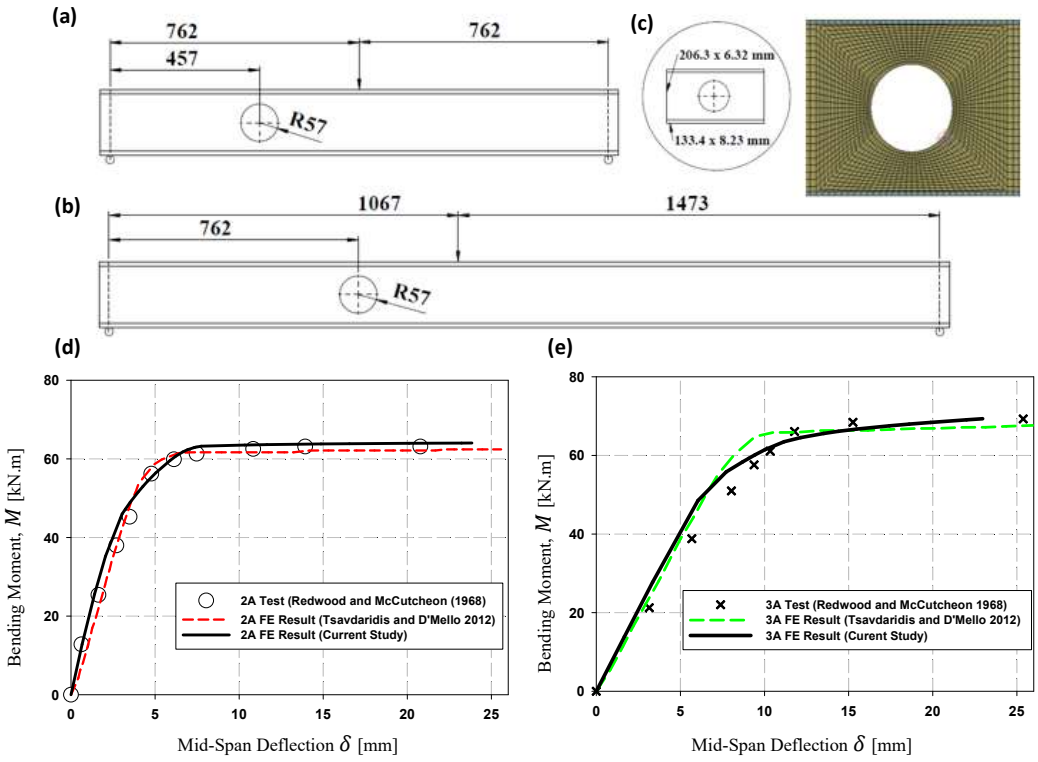

Figure 3: Gemoetrical configuration of (a) Beam 2A, (b) Beam 3A, (c) FE mesh around the opening, Comparison FEA results with the experimental results for (d) Beam 2A, (e) Beam 3A

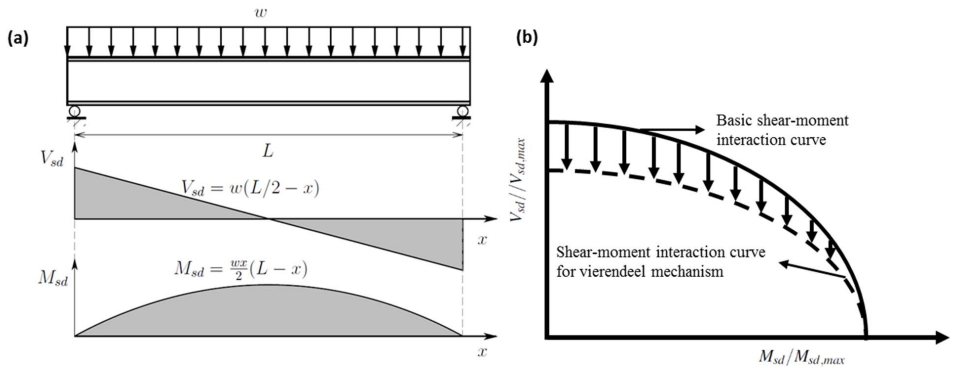

Figure 4: (a) Simply supported beam with distributed load (w), (b) Reduction due to Vierendeel mechanism

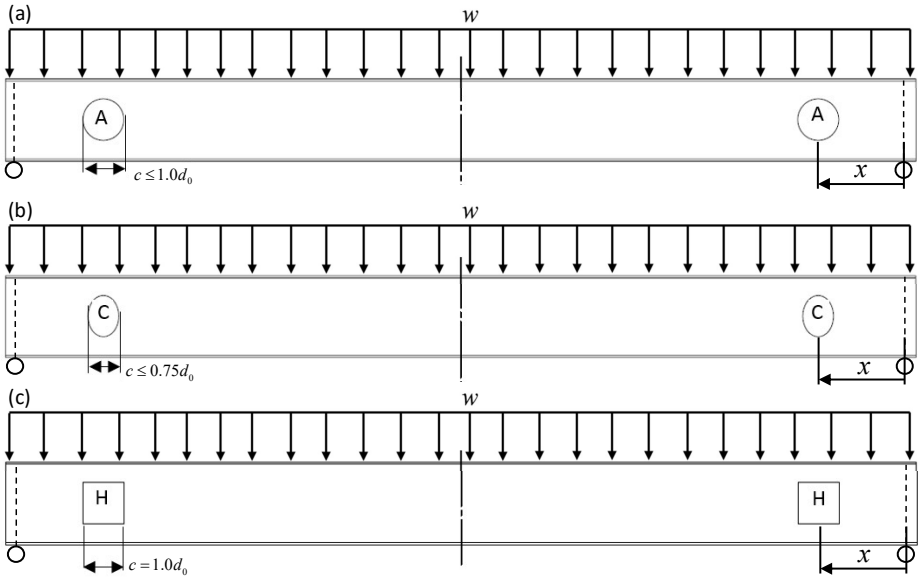

Figure 5: Web opening shapes and boundary conditions used in this study (a) opening A, (b) opening C and (c) opening H

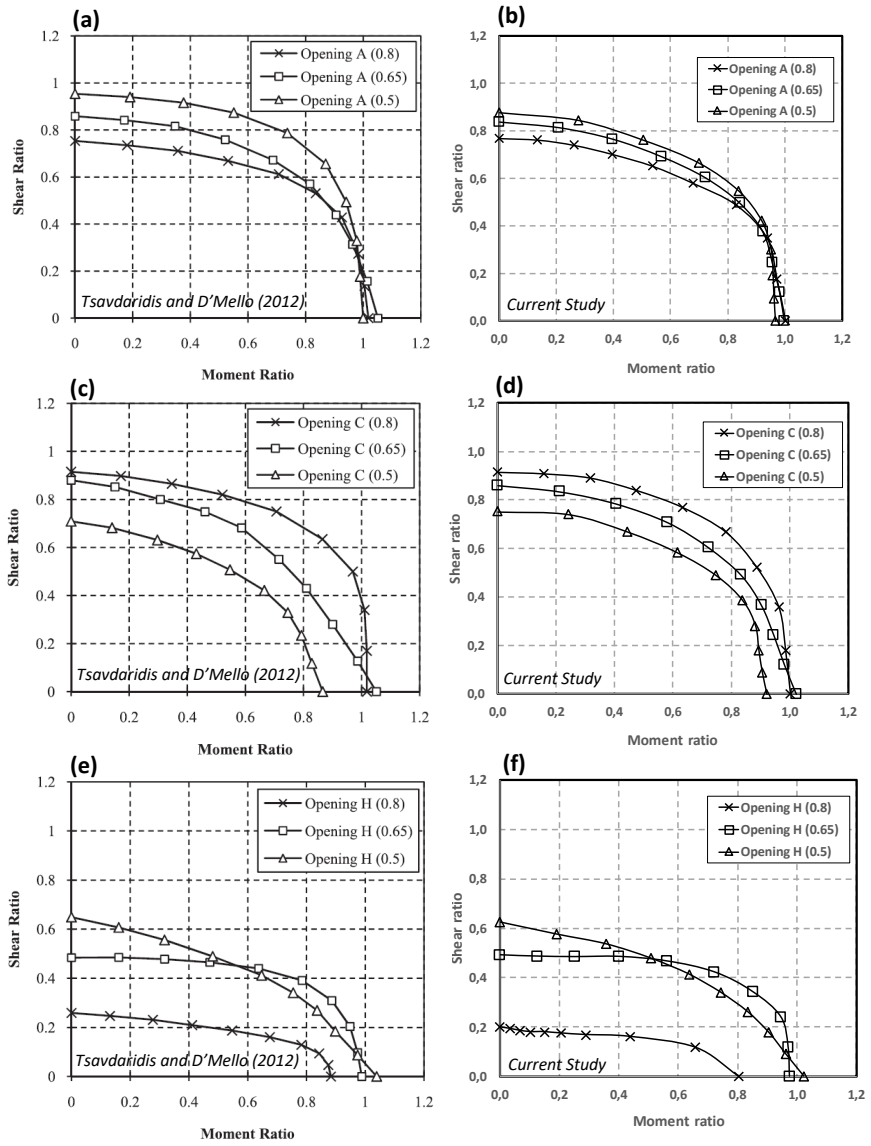

Figure 6: Comparison of Shear/Moment Interaction Curve Results (a) opening A (Tsavdaridis and D'Mello, 2012b), (b) opening A (Current Study) , (c) opening C (Tsavdaridis and D'Mello, 2012b), (d) opening C (Current Study), (e) opening H (Tsavdaridis and D'Mello, 2012b), (F) opening H (Current Study) (numbers in the legends refer to the ratio of web opening diameter to beam depth (d_0/h))

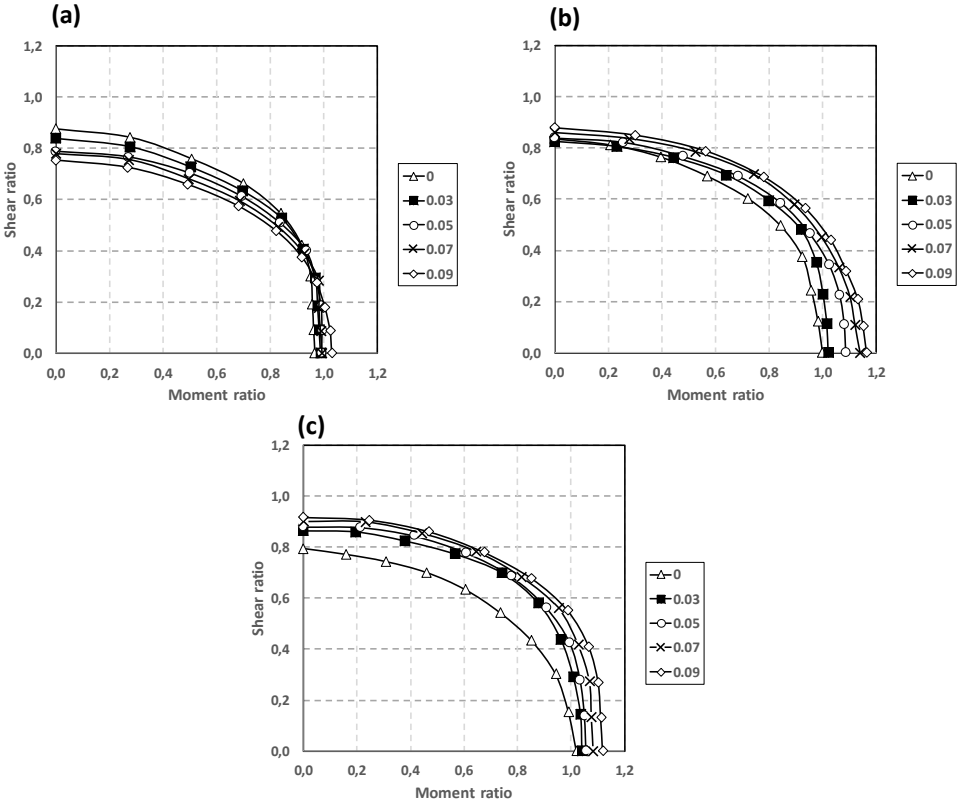

Figure 7: Shear/Moment Interaction curves for opening A (circlular type) ($h_s/t_w = 2$) (a) $d_0/h = 0.5$, (b) $d_0/h = 0.65$, (c) $d_0/h = 0.75$ (numbers in the legends refer to t_s/d_0)

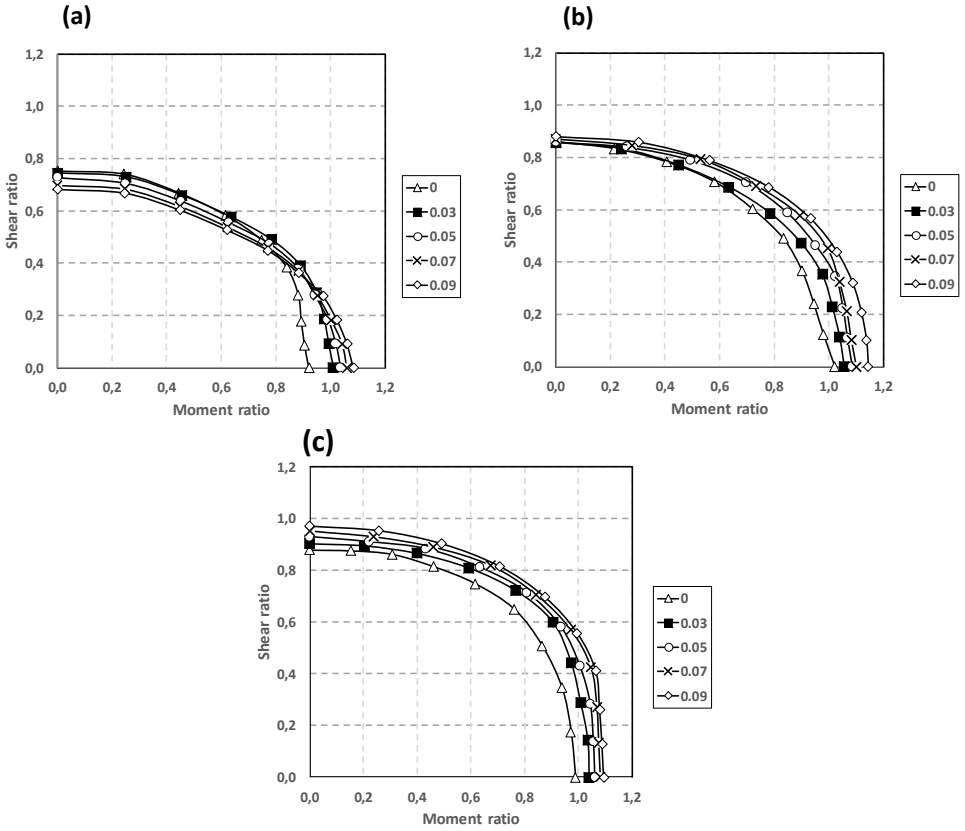

Figure 8: Shear/Moment Interaction curves for opening C (elliptical type) ($h_s/t_w = 2$) (a) $d_0/h = 0.5$, (b) $d_0/h = 0.65$, (c) $d_0/h = 0.75$ (numbers in the legends refer to t_s/d_0)

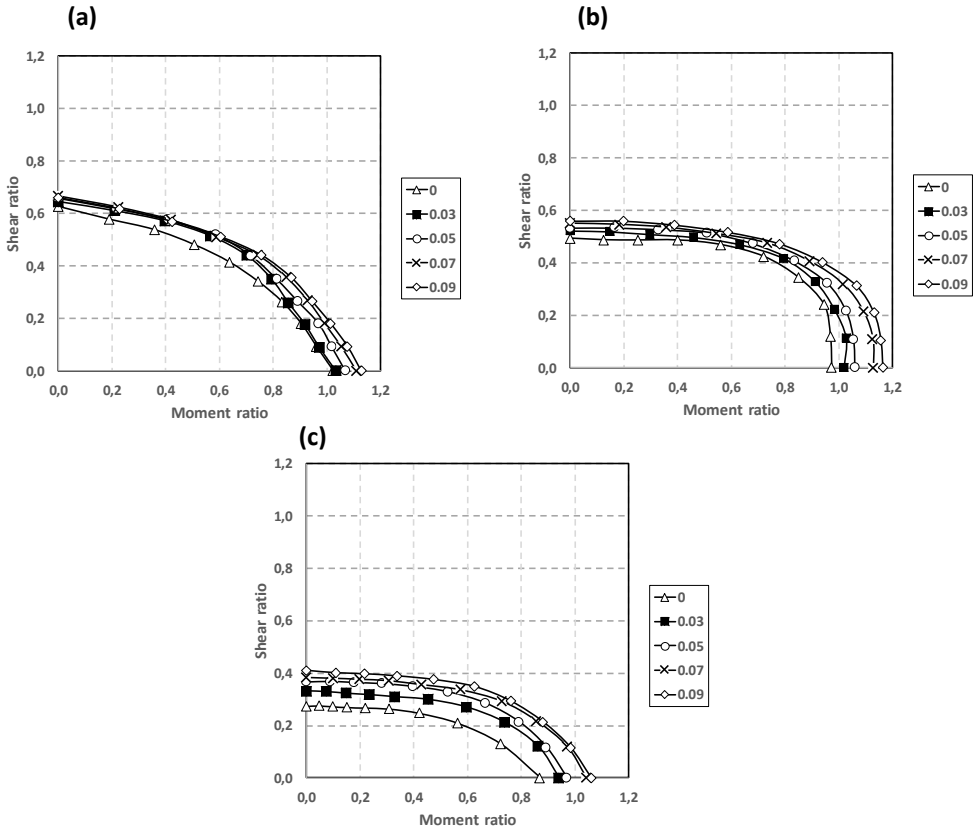

Figure 9: Shear/Moment Interaction curves for opening H ($h_s/t_w = 2$) (a) $d_0/h = 0.5$, (b) $d_0/h = 0.65$, (c) $d_0/h = 0.75$ (numbers in the legends refer to t_s/d_0)

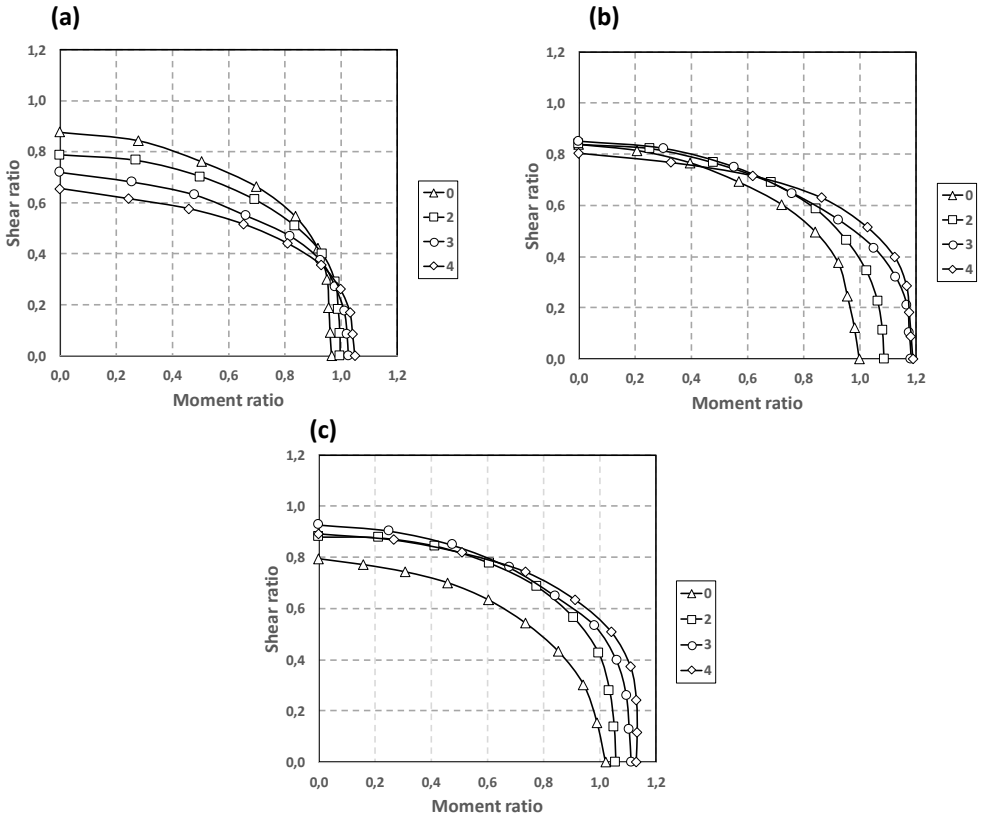

Figure 10: Shear/Moment Interaction curves for opening A ($t_s/d_0 = 0.05$) (a) $d_0/h = 0.5$, (b) $d_0/h = 0.65$, (c) $d_0/h = 0.75$ (numbers in the legends refer to h_s/t_w)

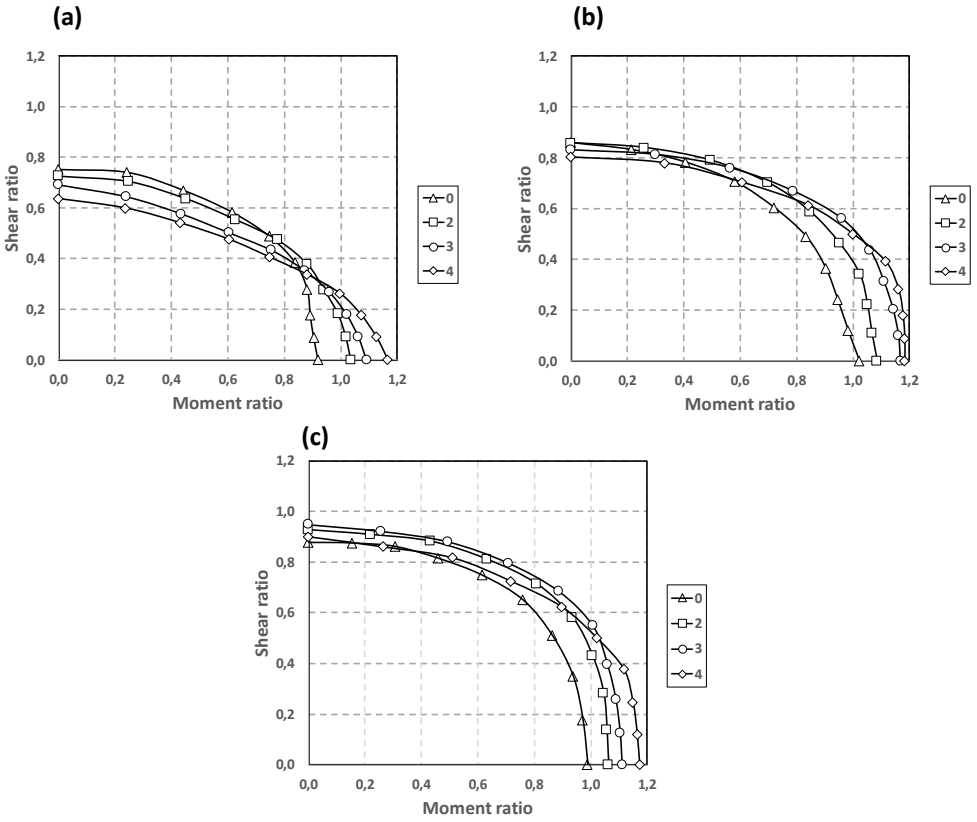

Figure 11: Shear/Moment Interaction curves for opening C ($t_s/d_0 = 0.05$) (a) $d_0/h = 0.5$, (b) $d_0/h = 0.65$, (c) $d_0/h = 0.75$ (numbers in the legends refer to h_s/t_w)

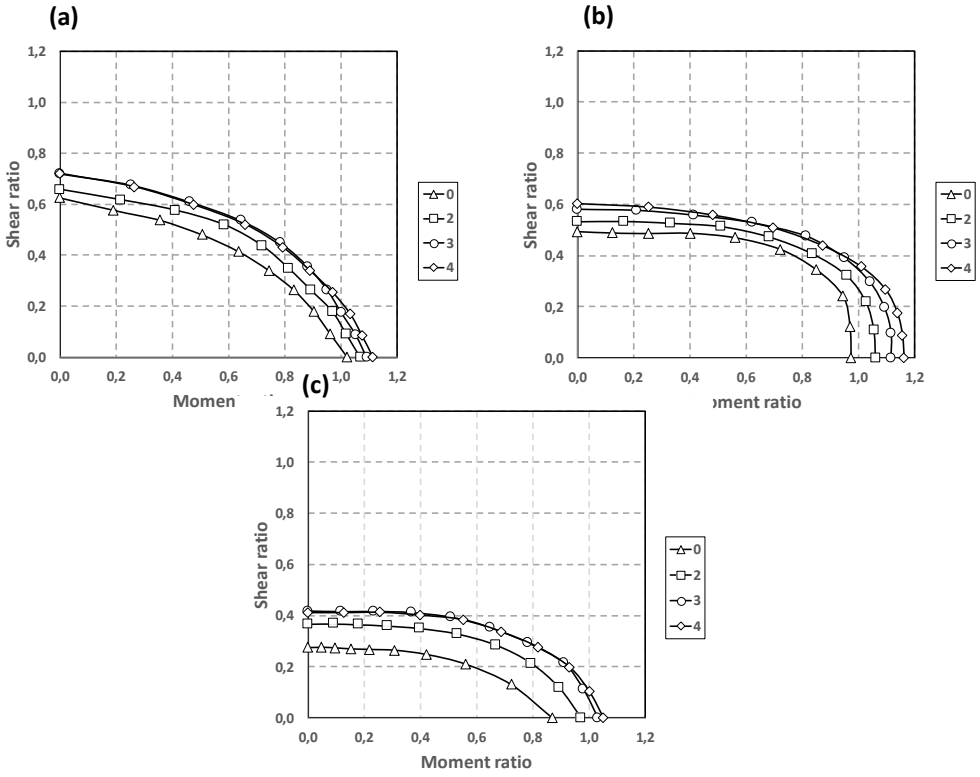

Figure 12: Shear/Moment Interaction curves for opening H f ($t_s/d_0 = 0.05$) (a) $d_0/h = 0.5h$, (b) $d_0/h = 0.65$, (c) $d_0/h = 0.75$ (numbers in the legends refer to h_s/t_w)

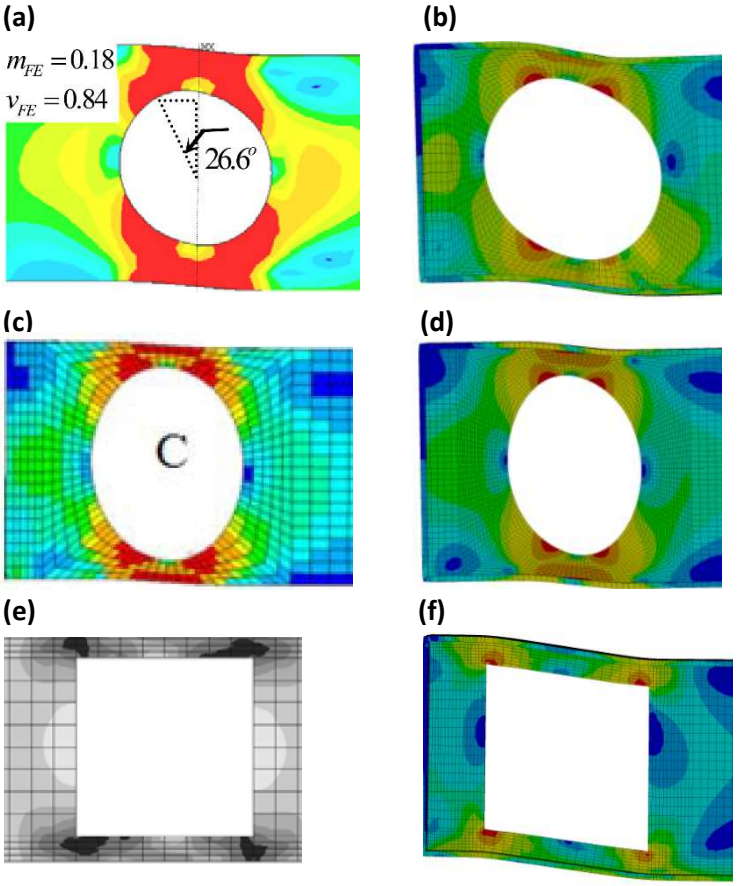

Figure 13: Comparison of yield patterns (a) opening A (Panedpojaman et al., 2015), (b) opening A (current study), (c) opening C (Tsavdaridis and D'Mello, 2012b), (d) opening C (current study), (e) opening H (Liu and Chung, 2003), (f) opening H (current study)

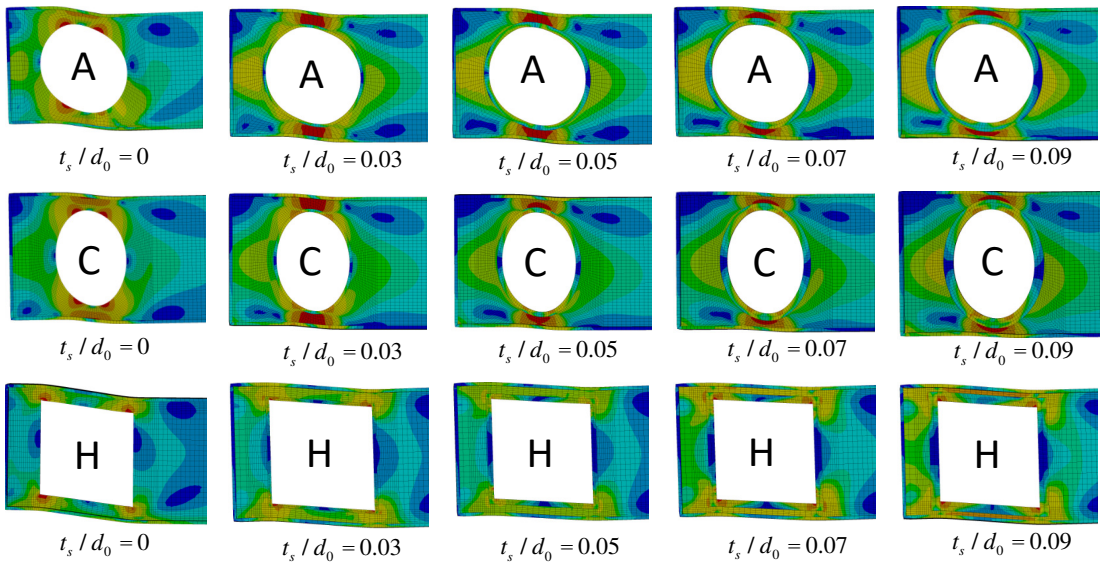

Figure 14: Deformed views of the beam (true scale, $h_s/t_w = 2$), for web opening position at $x = 284$ mm and $d_0/h = 0.75$

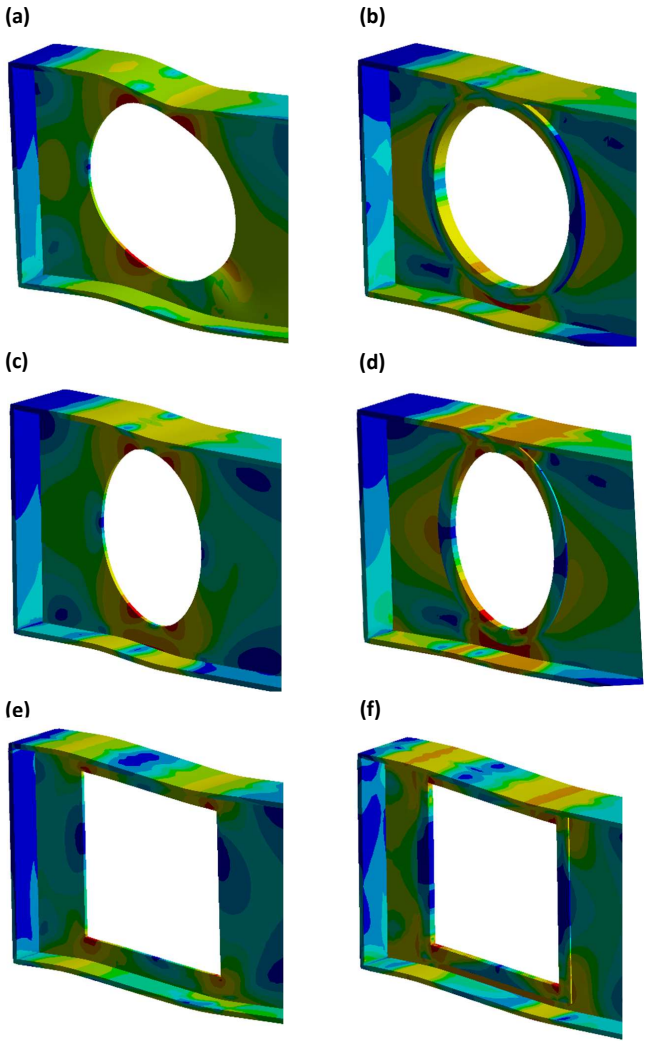

Figure 15: 3D deformed view of the von-Mises stress distributions at the web opening location ($x = 284$ mm) (a) opening A (unstiffened, $d_0/h = 0.75$), (b) opening A (stiffened, $d_0/h = 0.75$, $t_s/d_0 = 0.09$ and $h_s/t_w = 2$), (c) opening C (unstiffened, $d_0/h = 0.75$), (d) opening C (stiffened, $d_0/h = 0.75$, $t_s/d_0 = 0.09$ and $h_s/t_w = 2$), (e) opening H (unstiffened, $d_0/h = 0.75$), (f) opening H (stiffened, $d_0/h = 0.75$, $t_s/d_0 = 0.09$ and $h_s/t_w = 2$)

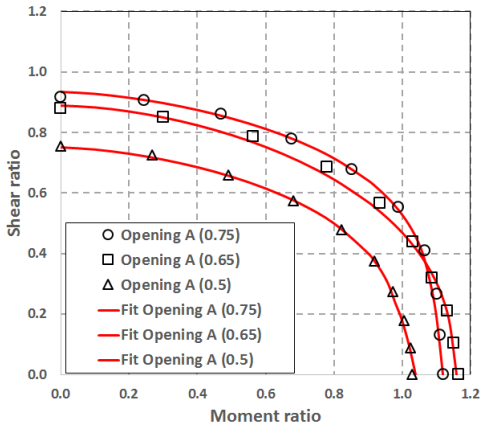

Figure 16: Fitted curve that is obtained by using Eq. (21) for the beam with the geometrical parameters $d_0 = 0.5h$, $0.65h$ and $0.75h$, $t_s/d_0 = 0.09$ and $h_s/t_w = 2$